Journal of Colloid and Interface Science 602 (2021) 480–489

Contents lists available at ScienceDirect

Journal of Colloid and Interface Science

journal homepage: www.elsevier.com/locate/jcis

Regular Article

Macroscopic rods from assembled colloidal particles of hydrothermally carbonized glucose and their use as templates for silicon carbide and tricopper silicide

Xia Wang [a], Wenming Hao [a,b], Peng Zhang [a], Anthony E. Szego [a], Gunnar Svensson [a], Niklas Hedin [a,*]

[a] Department of Materials and Environmental Chemistry, Stockholm University Svante Arrhenius väg 16 C SE 10691 Stockholm, Sweden
[b] School of Chemistry and Chemical Engineering, Taiyuan University of Technology 79# West Yingze Street CN 030024 Taiyuan, China

GRAPHICAL ABSTRACT

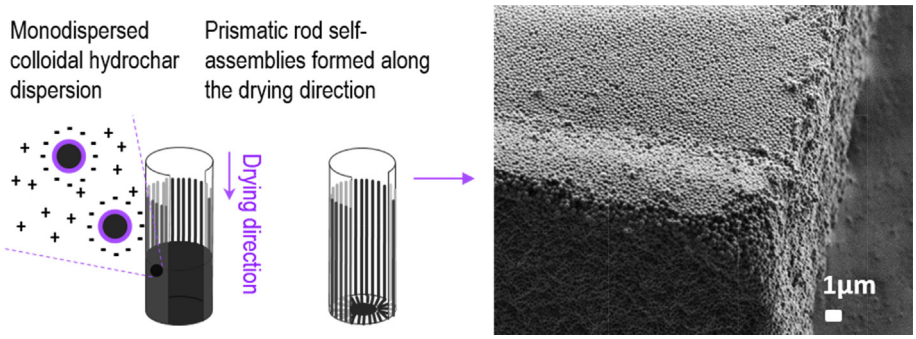

ARTICLE INFO

Article history:
Received 11 March 2021
Revised 1 June 2021
Accepted 2 June 2021

Keywords:
colloids
assembly
hydrothermally carbonization
monodisperse
templating
reactive infiltration
silicon carbide
hydrochar

ABSTRACT

Self-aggregated colloids can be used for the preparation of materials, and we studied long rod-like aggregates formed on the evaporation of water from dispersed particles of colloidal hydrochar. The monodispersed hydrochar particles (100–200 nm) were synthesized by the hydrothermal carbonization of glucose and purified through dialysis. During the synthesis they formed colloidal dispersions which were electrostatically stable at intermediate to high pH and at low ion strengths. On the evaporation of water, macroscopically large rods formed from the dispersions at intermediate pH conditions. The rods formed at the solid-water interface orthogonally oriented with respect to the drying direction. Pyrolysis rendered the rods highly porous without qualitatively affecting their shape. A Cu-Si alloy was reactively infiltrated into the in-situ pyrolyzed hydrochars and composites of tricopper silicide (Cu_3Si)-silicon carbide (SiC)/carbon formed. During this process, the Si atoms reacted with the C atoms, which in turned caused the alloy to wet and further react with the carbon. The shape of the underlying carbon template was maintained during the reactions, and the formed composite preparation was subsequently calcined into a Cu_3Si-SiC-based replica of the rod-like assemblies of carbon-based colloidal particles. Transmission and scanning electron microscopy, and X-ray diffraction were used to study the shape, composition, and structure of the formed solids. Further studies of materials prepared with reactive infiltration of alloys into self-aggregated and carbon-based solids can be justified from a perspective of colloidal science, as well as the explorative use of hydrochar prepared from real biomass, exploration of the compositional space in relation to the reactive infiltration, and applications of the materials in catalysis.

* Corresponding author.
E-mail address: niklas.hedin@mmk.su.se (N. Hedin).

https://doi.org/10.1016/j.jcis.2021.06.016
0021-9797/

1. Introduction

Assemblies of colloidal particles have properties that depend on the size, chemical composition, bulk structure, and crystallinity of the underlying colloidal particles [1]. Such assemblies typically form by the aggregation of monodispersed colloids, which in turn have been studied since the time of Faraday and his studies of colored gold sols [2]. The interest in studying dispersed and uniform colloids was initially academic and involved the quantification of physical properties or surface interactions, which were related to morphology, particle size, etc [3,4]. However, well-defined and dispersed colloidal particles have also become technically important in ceramics, catalysis, pigments, recording materials, medical diagnostics, etc [5–11].

When designing functional materials with controlled assembly of colloidal particles, it is useful and common to use spherical and monodispersed particles [12]. During the assembly, a suitable combination of repulsive and attractive intraparticle interactions is needed [13], and the assembly can be directed by external fields or proceed by pure self-assembly. Well-controlled assembly of colloidal particles into macroscopic objects has been observed for many classes of matter, which include silica [14], metals, [15,16] and polymers [17,18]. (It should also be noted that monodispersity is not a necessary condition, as polydispersed colloids can also, sometimes, form monodisperse supraparticles) [16]. Very few studies (if any) have been focused on the formation and use of macroscopic assemblies of carbon-based colloidal particles. This lack of attention is surprising as carbon-based materials are relevant for catalysis, manufacturing, electrochemistry, etc [19–24].

A rediscovered class of carbonized materials are the hydrochars which are prepared by the hydrothermal carbonization (HTC) of biomass or simple sugars [25]. HTC is performed at elevated temperatures (180–250 °C) and autogenous pressures, via dehydration and polymerization reactions, and phase-separation processes [26,27]. After the synthesis, the hydrochar particles coexist with molecules in a combination of aqueous and sorbed phases. Hydrochar particles prepared from the HTC of simple sugars consist on crosslinked polymers rich in furan groups, and they have a composition which is similar to peat or lignite [28]. When prepared from the HTC of glucose, the hydrochar particles are typically spherical, reflecting that a liquid–liquid phase separation has occurred during the preparation [25,29,30]. Monodispersed and spherical hydrochar particles can be synthesized as was established by Wang et al. [31] and studied by others [1,32,33]. Monodispersed particles of hydrochar have been prepared from sugar, starch, maltose and glucose.

Here, we present a study on the colloidal chemistry of dispersed and purified uniform particles of hydrochar, and show that such particles assemble into macroscopic rods during the evaporation of water at the interface of glass or polypropylene. We also report on how these rod-like and carbon-based colloidal assemblies could be used as templates for the preparation of materials based on silicon carbide (SiC) and tricopper silicide (Cu_3Si) by reactive infiltration of a copper-silicon (Cu-Si) alloy and subsequent calcination.

2. Experiments and characterization

2.1. Hydrochar synthesis

Hydrochar was prepared by the HTC of glucose (Sigma-Aldrich, 97.5–102.0%). Glucose was dissolved in water and transferred into Teflon™ lined autoclaves, which were sealed and placed in a preheated oven at a temperature of 175 or 195 °C for 1 or 2 h. After preparation, the autoclaves were rapidly cooled down in cold water. (**Caution:** quenching autoclaves in this manner is non-standard and may be hazardous.) 30-ml autoclaves were used. Four parameters were optimized in a set of 2^4 = 16 experiments using a design matrix and the principle of design of experiments. The parameters used in the design were the glucose concentration (0.3 or 0.5 mol/dm^3), filling ratio (70 or 90%), temperature (175 or 195 °C) and reaction time (1 or 2 h), see Table S1-S2 for the detailed conditions of preparations of the 16 experiments. The preparations were named with the level of the four investigated factors (parameters), and when they were all high, the preparation was called as 1111. Following the results from the optimization by experimental design, all the other syntheses were performed at 195 °C, with a filling ratio of 75% and for 2 h. For these experiments somewhat smaller autoclaves were used with volumes of 20–24 ml. The CH0.5 sample was prepared by the HTC of glucose with a concentration of 0.5 mol/dm^3, and the CH0.3, CH0.5, CH1.0, and CH1.5 by the HTC of glucose solutions with concentrations 0.3, 0.5, 1.0 and 1.5 mol/dm^3 respectively.

2.2. Hydrochar purification

The crude brown hydrochar dispersions prepared by the HTC of glucose were purified by dialysis. Dispersions were introduced in sealed dialysis tubings (DTs) and placed in contact with deionized water or other water-based permeates with different pH or ionic concentrations. Permeates were regularly changed until the conductivities of the permeates close to the DT became similar to that of the bulk of the permeate, and stable. A DT type with a 14000 Da cut-off, was used (MEMBRA-CEL® MD77). The conductivity was measured with an XS COND 70 + pH/conductivity meter. Liquid-state ^{1}H NMR spectroscopy was used to identify compounds in the aqueous phases before and after purification and spectra are shown in Figure S7. The dialyzed CH0.3, CH0.5, CH1.0, and CH1.5 dispersions were named as d-CH0.3, d-CH0.5, d-CH1.0 and d-CH1.5.

For the purpose of comparison, samples were purified by centrifugation and redispersion in addition to dialysis. In these preparations, the crude dispersions collected from the HTC were subjected to centrifugation at a rate of 9000 rpm for 15 min. A LMC-4200R laboratory refrigerated centrifuge was used. The liquid was poured off, distilled water was added, and centrifugation was performed again; this process was repeated and three centrifugations were performed.

2.3. Evaporation of water and formation of rods

Water was evaporated from the dispersions at a temperature of 80 °C using a Thermo Scientific oven or a heated oil bath. Evaporation was performed from dispersions in glass vials (1.5 cm and 2.6 cm in diameter), polypropylene vials (2.5 cm in diameter), a glass petri dish, a Teflon liner, and an aluminum metal surface. For the sample dried on a glass petri dish, the drying was performed at room temperature in a fume hood.

2.4. Redispersion of the hydrochar particles

To test the redispersibility of the hydrochar particles, the hydrochar dispersions prepared at different pH values (d-CH0.5pX) were first redialyzed using deionized water as the permeate, and then the dispersions/suspensions were subsequently sonicated for 2–30 min with a Bandelin sonicator at 320 W. Similar redispersion tests were performed at different concentrations of NaCl. The macroscopic rods were sonicated with the same amount of water and dried (or not dried) before the tests of redispersibility. If the dispersion appeared visibly uniform and brownish, similar to the purified dispersion d-CH0.5, and without observable large particles, then the redispersibility was marked down with a yes (Y),

otherwise with a no (N). We also tested the redispersibility using centrifugation with water, ethanol and acetone.

2.5. Zeta potential measurements

For studies of the pH-dependent zeta potential, a series of samples were prepared at different pH values (2–12) using dialysis. Permeate baths of deionized water with different pH values were prepared with either HCl (VWR, 36.1%) or NaOH (VWR, 99.1%). The ion strengths of these preparations were comparably low. Aliquots of the purified sample d-CH0.5 were subjected to dialysis in such baths, and the permeate was regularly changed until the conductivity close to the DT was similar to that of the permeate and stable. These purified and pH controlled dispersions were called d-CH0.5p2, d-CH0.5p4, d-CH0.5p10, and d-CH0.5p12 (pX denotes the pH).

Zeta potentials were determined for dispersions at different pH values with a Zetasizer Nano-ZS (Malvern Instrument Ltd.) at 25 °C. The colloidal hydrochar dispersions were diluted with deionized water before the measurements of the zeta potentials. The new pH values were recorded. The disposable folded capillary cells were cleaned properly and filled gently with the dispersions using disposable syringes. Care was taken to assure that no air bubbles were introduced in the cells before the zeta potential values were determined. Aliquots of an aqueous solution of 1.0 mol/dm^3 of HCl was also added to further adjust the pH value of the sample d-CH0.5p2, to assure that the zeta potential had reached a positive value. This additional preparations ensured that the determination of the isoelectric point could be conducted.

2.6. Colloidal stability tests

The purified dispersions d-CH0.5 were centrifuged, filled into DTs, and subjected to two-liter baths as permeates with NaCl (VWR, 99.8%) concentrations of 0.5%, 1.0%, 1.5% and 2.0% (w/w) corresponding to 86, 171, 257 and 342 mmol/dm^3. The preparations were named as c-CH0.5–86, c-CH0.5–170, c-CH0.5–260 and c-CH0.5–340. The preparations were subsequently transferred to vials, observed, and photographed for three weeks to identify destabilization of the dispersions by sedimentation.

2.7. Pyrolysis and reactive infiltration

The macroscopically large rods of assembled hydrochar particles were pyrolyzed at temperatures of 600, 800, and 900 °C for 2 h. The pyrolysis was conducted in a N_2 (≥99.9%) atmosphere using a Carbolite MTF Wire Wound Single Zone Tube Furnace (with a 25-mm inner diameter).

Reactive infiltrations of a Cu-Si alloy into the macroscopically large rods of assembled hydrochar (d-CH0.5) were conducted under conditions of in-situ pyrolysis and reactive infiltration in an Ar atmosphere. The d-CH0.5 rods and a Cu-Si alloy (4–12 at.% of Cu) were used with a mass fraction of hydrochar:alloy = 1:1.5. The alloy was positioned over a loose pack of the macroscopic rods of d-CH0.5. The temperature was increased to 1300 °C with a rate of 5 °C/min and kept at the target temperature for 1 h. The sample was collected and named Cu_3Si-SiC/carbon. A part of the Cu_3Si-SiC/carbon was picked out for calcination in technical air at 550 °C for 6 h in a muffle oven and was called Cu_3Si-SiC after calcination.

2.8. Characterization

The monodispersity and hydrodynamic diameters were determined by dynamic light scattering (DLS) for the dispersions using a Zetasizer Nano-ZS (Malvern Instrument Ltd.) at 298 K. Powder X-ray diffraction (PXRD) data were collected on a PANalytical X'Pert Pro diffractometer using a Cu Kα radiation (λ = 1.5418 Å). The morphology of the macroscopically large self-assembled rods, the pyrolyzed rods, and the materials prepared by reactive infiltration (the Cu_3Si-SiC/carbon and Cu_3Si-SiC) were studied using field emission scanning electron microscopy (SEM). A JEOL JSM-7000F was operated at 1–15 kV with a gentle beam and a table top SEM (Hitachi, TM3000) was also used under its analysis mode. SEM images were recorded in a secondary electron mode. Elemental compositions were determined by SEM using energy–dispersive X-ray spectroscopy (EDS). Transmission electron microscopy (TEM) studies were performed with a JEOL JEM-2100F microscope operated at 200 kV. For sample preparation in relation to TEM, the hydrochar rod sample (d-CH0.5) was slightly grinded and dispersed onto a holey carbon coated copper grid directly. Another TEM sample of d-CH0.5 was prepared by an ultra-microtome sectioning approach.

The surface areas and porosities were analyzed with a Micromeritics ASAP 2020 instrument using pressure dependent N_2-adsorption data recorded at −196 °C. Samples were subjected to deep dynamic vacuum first at 100 °C for 1 h and then at 180 °C for 4 h before proceeding with the N_2 adsorption/desorption experiments. The surface areas were determined using the Brunauer-Emmett-Teller (BET) theory with N_2 adsorption data. Special care was taken to select the pressure regime for the BET analysis for the highly microporous pyrolyzed sample. Pore size distributions were calculated from the N_2 adsorption data by a density functional theory (DFT) method assuming a slit-shaped pore geometry.

3. Results and discussion

3.1. Millimeter-sized rods of assembled hydrochar particles

Macroscopically large millimeter-long rods of assembled hydrochar particles formed on the slow evaporation of water at 80 °C in glass and polypropylene vials. The photograph in Fig. 1a *top* shows the macroscopic dimensions of the rods. Prismatic rods formed on the evaporation of water at an elevated temperature in glass vials (2.1–3.5 g/dm^3 for d-CH0.5) for all tested particle concentrations. The rods formed vertically at the curved inner surface of the vials, orthogonal to the slowly moving liquid surface, as is illustrated in Fig. 1a *bottom*. On drying in a flat glass petri dish (8.0 cm in diameter), rods formed on the bottom of the vial, diverging towards the center, orthogonally with respect to the moving liquid front; no rods formed close to the center. When the same dispersion (d-CH0.5) was dried at room temperature, no rods formed (Figure S2a); however, the macroscopic pieces that formed consisted of comparably well-organized and assembled hydrochar (Figure S2b). Rods also formed on the evaporation of water from hydrochar dispersions in polypropylene vials (Figure S2c) but not in Teflon™ or aluminum containers (Figure S2d–e). The sides of the rods that had been in contact and parallel with the glass surface were considerably smoother than the other sides, as can be observed in the SEM images (Fig. 1b *top* and *bottom*). That the rods consisted of densely packed and relatively well-organized particles is evident from SEM images such as those in Fig. 1b *bottom* and c. The normally solid form of the hydrochar particles is displayed in the TEM image of Fig. 1d, and in the TEM images of ultramicrotomed preparations (Figure S1). For the ultramicrotomed rods, most of the hydrochar particles were solid, however, occasionally hollow ones were observed.

The mechanisms of rod formation can be related to findings for other classes of dispersed particles. Fojtik et al. has, for example, shown that negatively charged nanoparticles can assemble into large objects [34], and it has been shown that during evaporation,

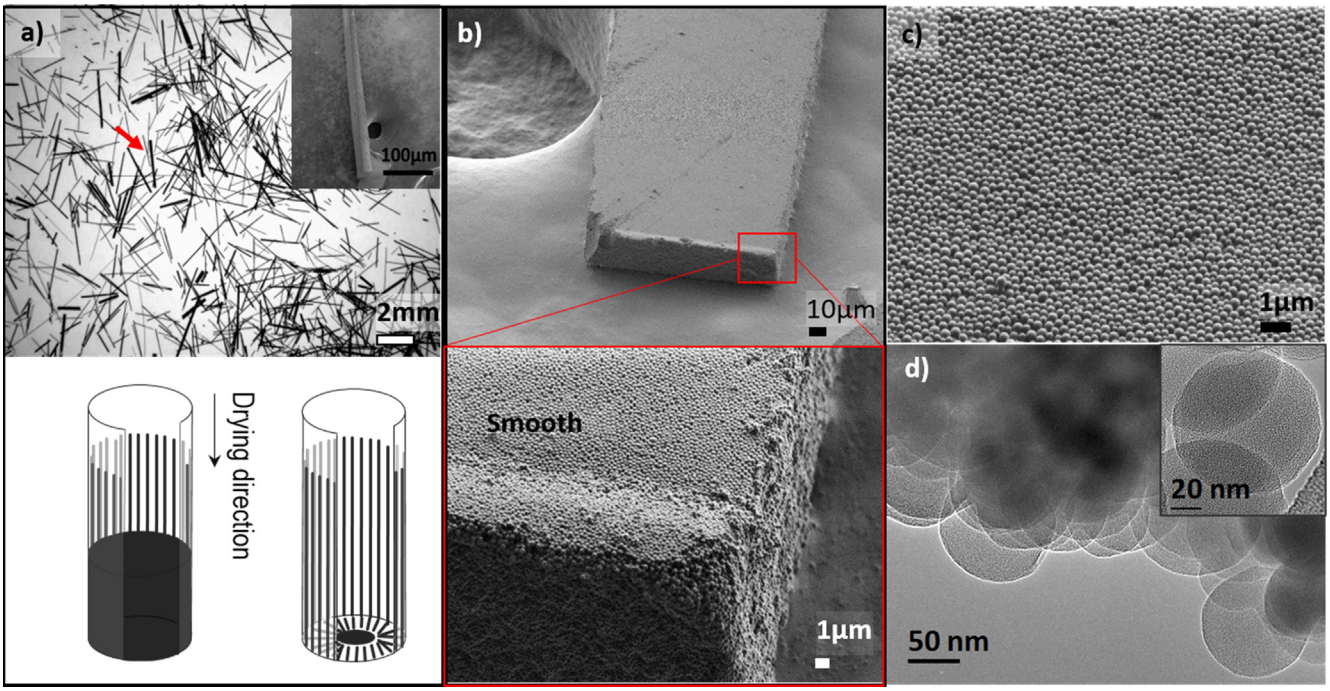

Fig. 1. a) *top* A photograph with an insert SEM image displays rods that formed at the glass interface of a vial on the evaporation of water from a purified dispersion of highly monodisperse colloidal hydrochar. a) *bottom* A scheme shows the rods forming on the curved inner surface of a glass vial along the drying direction. b) *top* The SEM image shows the smooth surface and edge-cutting end of the self-assembly and b) *bottom* A display of well-arranged particles on one of the smooth faces, and two rough faces of the self-assembly. c) The SEM image shows the well-organized array of the self-assembled hydrochar rod sample, and d) The TEM image is from a broken edge of a rod and the insert displays one typical hydrochar particle. The dispersion was prepared with 0.5 mol/dm^3 of hydrothermally carbonized glucose at 195 °C for 2 h and purified by dialysis (sample 1111). (1111 stands for the values of the experimental design matrix, see Table S1 and S2.)

particles can assemble into large structures under conditions of strong and anisotropic interparticle interactions [35]. It is noted that self-assembly of colloidal crystals of monodisperse silica or PMMA particles is governed by a delicate balance between long-range electrostatic repulsive and short-range attractive interparticle interactions [36]. A similar balance of interparticle interactions has likely been active during the formation of the rods, which is also supported by the study of the colloidal stability presented later on in this text. It has also been observed for materials other than hydrochar that nanoparticles may assemble as lines during evaporation [37]. Such macroscopic lines of particles adhere to the surface and normally form horizontally [38,39], but they can also form vertically, in a manner sometimes ascribed to fingering instabilities [40–42]. In this study, vertically oriented lines of assembled particles formed at the interface (c.f. Fig. 1b) and ultimately disadhered in the form of macroscopic rods.

As was mentioned already, monodispersed hydrochars have been synthesized by others [31,33], but in those studies no attention was given to the purification of the dispersions. Large amounts of unreacted glucose and other dissolved molecules were present in the crude dispersions of these studies. The dispersions were purified by dialysis or centrifugation/redispersion. A purification that was shown to be necessary for the directed assembly of macroscopic rods on the evaporation of water. To achieve highly monodisperse hydrochar, we used a multi-parameter optimization with respect to the reciprocal polydispersity index (1/PDI), determined by DLS. The particle diameters were larger when determined by DLS than by scanning electron microscopy (SEM), see Figure S3. Details on the optimization is given in Table S1–S2, and Figure S4. The time and temperature used for synthesis affected the monodispersity positively, and a high monodispersity (1/PDI $\geq$ 10.00) was reached over a wide range of glucose concentrations used for the HTC (0.3–1.5 mol/dm^3). Particle sizes and PDIs are presented for these hydrochar dispersions in Table 1. We know from other studies that the concentration of glucose exerts a control of the particle size and size distribution of the hydrochar formed during HTC [33]. At high concentrations of glucose, (1.5–3.0 mol/dm^3), large and relatively polydisperse hydrochar particles (>500 nm) formed, which was consistent with literature data [31]. When the underlying hydrochar particles were polydisperse, irregular morphologies of the macroscopic assemblies formed in most cases on the evaporation of water. However, for some few instances when the hydrochar particles were purified by centrifugation rather than by dialysis, we observed the formation of rods on water evaporation even when the 1/PDI was < 5 (Figure S2f). The sides of the macroscopic rods were rougher for these preparations as compared with those formed from water evaporation for dialysed preparations. For the dispersion d-CH0.5, the particle diameter (as determined by DLS) was 148 ± 2 nm after purification by dialysis and 236 ± 3 nm after purification by centrifugation. The corresponding PDIs were 0.05 and 0.26. The relatively high PDI for the sample purified by centrifugation was consistent with (some) pseudo-aggregates of colloidal particles being present in the dispersion. (In Table S5, the average hydrodynamic diameters are presented for the particles in hydrochar dispersions purified by centrifugation with water, or with other media and then redispersed in water.) Note that others have shown that polydispersity is not a priori needed for the formation of defined and regular aggregates on particle assembly [16,43].

When the hydrochar dispersion comprised large particles, the axial ratios of the rods formed on water evaporation were reduced (Figure S5a–c). A reflective structural color on the smooth sides of the prismatic rods (inserts of Figure S5a–c) was observed, and the colors varied with the size of the underlying hydrochar particles. A thin film with reflective colors floating in the hydrochar dispersions was also observed (Figure S5d) [44]. Rods formed on the

Table 1
The influence of concentration to the monodispersity and particle size, at a constant temperature (195 °C), filling factor (75% in 20–24 ml autoclaves) and time (2 h).

Sample	$C_{Glucose}$/mol/ dm^3	PDI**	1/PDI	Mean Particle diameter/nm (DLS results)
d-CH0.3	0.3 ± 3.2E-15*	0.047 ± 0.021	21.3	122.6 ± 0.1
d-CH0.5	0.5 ± 5.6E-17	0.050 ± 0.042	20.0	147.9 ± 1.5
d-CH1.0	1.0 ± 5.8E-12	0.044 ± 0.040	22.7	251.9 ± 4.0
d-CH1.5	1.50 ± 1,5E-11	0.100 ± 0.028	10.0	474.1 ± 17.0

* Errors estimated on three values for each.
** PDI of diluted dispersions. d-CHX denotes the dialyzed colloidal hydrochar prepared by hydrothermal carbonization of glucose at concentrations of X mol/dm^3. Based on the optimized time and temperature of the experimental design, d-CH0.5 was similar to sample 1111, except that the filling ratio was 75% instead of 90% and that a 20–24 ml autoclave was used. d-CH0.5 is the 'standard' sample for many of the following experiments. For PDI and DLS tests, 10 measurements with 10 runs for each were done for each dispersion.

evaporation of water at the glass interface at an intermediate pH range (4.1–9.5) and irregular shapes formed at lower or higher pH values (2.1 or 12.1), see Figure S6. On the evaporation of water from a dispersion of hydrochar at a pH = 2.1, the lack of rods formed was ascribed to a non-sufficient level of electrostatic stabilization of the dispersion (see Table 2). On the evaporation of water at a pH = 12.1, the absence of rods formed was ascribed to the silica chemistry at the interface (being related to interactions or chemical reactions). Information on the monodispersity, self-assembly, redispersibility in water after the dialysis, and if the macroscopic rods formed on the evaporation of water is presented in Table 2. Note that the non-dried rods could be redispersed into colloidal hydrochar by dialysis with deionized water but the dried rods could not be redispersed.

3.2. Colloidal properties of the hydrochar dispersions

Zeta potentials (in Fig. 2) of the particles in dialyzed hydrochar dispersions were significantly negative at most pH values. The corresponding isoelectric point was 0.78. The crude hydrochar dispersion had a pH = 2.6, and hydrochar particles have acid surface groups [45]. At a pH > 3.4, the zeta potential was < – 40.0 mV, and the values are also listed in Table S3. Such low values typically provide electrostatic stability to the dispersions. The pH range for the stable dispersions was pH = 4.1–9.5, and the zeta potential allows for assessing the electrostatic stability for colloidal dispersions. They are typically stable when the zeta potential is high or low enough, at moderate ion strengths [46–48]. We did not find any literature on the pH-dependent zeta potentials or the corresponding isoelectric points for particles in hydrochar dispersions. Other studies have reported on moderately low zeta potentials of hydrochar particles, with reported values of – 15 to – 20 mV [45,49]; however, in those studies the dispersions were not purified. Noteworthy is that the pH range for electrostatic stability of the dispersions coincided with the pH range for rod formation on the evaporation of water from the dispersions.

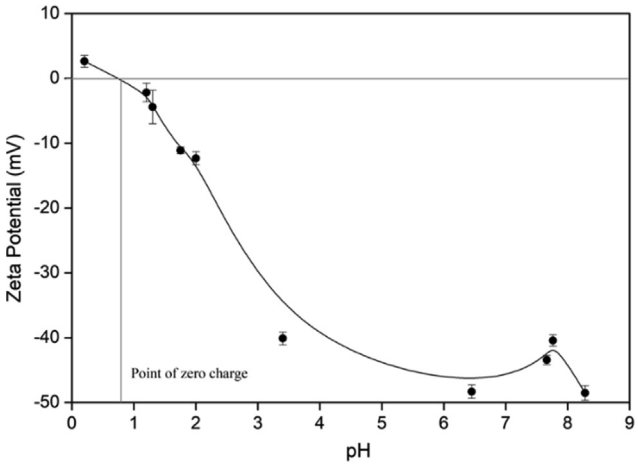

Fig. 2. The zeta potentials of particles in a dispersion (d-CH0.5) of colloidal hydrochar particles prepared by hydrothermal carbonization of glucose and purified by dialysis as a function of the pH value. d-CH0.5 denotes a dispersion of hydrochar prepared by hydrothermal carbonization of glucose at concentrations of 0.5 mol/dm^3 and purified by dialysis. 3 measurements with 5 runs for each were done for each dispersion.

Within the DLVO theory [24,50] colloidal dispersions are destabilized by reducing the double-layer repulsive interaction by increasing the ion strength of the dispersions [51–53]. Such destabilization, on increasing the ionic strength (here with NaCl addition), was observed for the hydrochar dispersions. Photographs of the dispersions and destabilized dispersions are presented in

Table 2
Colloidal features of dispersions of spherical hydrochar particles prepared by hydrothermal carbonization of glucose, and especially the influence of the pH of the permeate used for the purification by dialysis.

Sample	pH			Dialysis* for 48 h		Left to stand still for one week after dialysis		Stability** / Rods or not	Redispersbility in H_2O ***/ Prismatic rods or not	Sphere size/nm
	Permeate	Dispersion		1/PDI	PDI	1/PDI	PDI			DLS(48 h dialysis)
		Before dialysis	After dialysis							
d-CH0.5p2	2.1 ± 0.01	2.6 ± 0.01	2.2 ± 0.01	11.8	0.085 ± 0.017	3.4	0.291 ± 0.013	N/N	Y/N	131.0 ± 0.9
d-CH0.5p4	4.1 ± 0.01	2.6 ± 0.01	4.0 ± 0.06	17.2	0.058 ± 0.014	14.5	0.069 ± 0.033	Y/Y	Y/Y	141.1 ± 0.8
d-CH0.5	Deionized H_2O	2.6 ± 0.01	4.6 ± 0.01	15.9	0.063 ± 0.026	38.5	0.026 ± 0.017	Y/Y	-/Y	144.3 ± 2.3
d-CH0.5p10	9.5 ± 0.01	2.6 ± 0.01	5.8 ± 0.04	21.3	0.047 ± 0.023	20.8	0.048 ± 0.021	Y/Y	Y/Y	130.3 ± 1.0
d-CH0.5p12	12.1 ± 0.02	2.6 ± 0.01	11.2 ± 0.02	13.9	0.072 ± 0.015	25.0	0.040 ± 0.027	Y/N	Y/Y	189.7 ± 2.5

* Proceeded in the solution with the corresponding pH. d-CHXpY denote hydrochar dispersions prepared by hydrothermal carbonization of glucose at concentrations of X mol/dm^3 and subjected to dialysis with respect to a permeate at a pH = Y. For PDI and DLS tests, 10 measurements with 10 runs for each were done for each dispersion.
** If the dispersion does not sediment after one week, then it is stable(Y), otherwise it is not (N).
*** Dialyzed again in deionized water and then sonicated. Errors for the pH values are estimated on two values for each

Fig. 3. Stable dispersions were observed for NaCl concentrations < 100 mmol/dm^3. At higher concentrations, precipitation and sedimentation were observed.

For concentrations of NaCl > 260 mmol/dm^3, the dispersions were destabilized after two days. After three weeks, a concentration of NaCl > 170 mmol/dm^3 was sufficient to destabilize the dispersions. (In Table S4, the zeta potential values and average hydrodynamic diameters are listed for these dispersions).

3.3. Pyrolysis of the hydrochars into carbons

The macroscopic structure of the rods and the spherical shape of the underlying particles were preserved after pyrolysis in N_2, as can be seen from the SEM images for the sample 1111 in Fig. 4 (compare also with Fig. 1). The average particle diameter decreased by 14.4% (from 257 to 220 nm) upon pyrolysis at 600 °C for 2 h. Pyrolysis was also conducted at 800 and 900 °C for 2 h, and the rod morphologies and the spherical shapes of the underlying particles were preserved. The pyrolysis at 800∘C yielded 42% pyrolyzed rods from the hydrochar. (Note that the dispersion used for preparing sample 1111 was synthesized using very similar HTC conditions as the ones used for d-CH0.5. A higher filling ratio and slightly differently sized autoclave were used.)

The surface area and porosity of the rod-like hydrochar and pyrolyzed hydrochar (800 °C for 2 h) were determined; corresponding adsorption and desorption isotherms for N_2 and pore width distribution curves are displayed in Fig. 5. For the hydrochar, the isotherm was of type V in the low-pressure regime (following the classification of the International Union of Pure and Applied Chemistry) but it had a significant uptake in the high p/p_0 range with a hysteresis loop at p/p_0 = 0.9–1.0, which is typical for a meso- and macroporous structure. For the pyrolyzed hydrochar, the isotherm was of type II, as shown in Fig. 5a, and the gradient of the adsorbed amount of N_2 with respect to pressure was high for low and high values of p/p_0. These trends, and the hysteresis loop at p/p_0 = 0.8–1.0 are typical for a combination of micro-, meso- and macrospore structure with more abundant porosity than for the hydrochar. The specific pore volumes and pore surface areas are presented in Fig. 5b–c. Pyrolysis generated pores within the spherical particles < 40 Å and mainly pores < 10 Å, as is shown in Fig. 5b–c. These small pores were related to voids formed during decomposition and crosslinking of the hydrochar during pyrolysis. Pores > 100 Å were observed for both the hydrochar and the pyrolized hydrochars. The pyrolized hydrochar had a large fraction of medium sized pores at around 250 Å, which was tentatively related to the shrinkage of the spherical particles during pyrolysis.

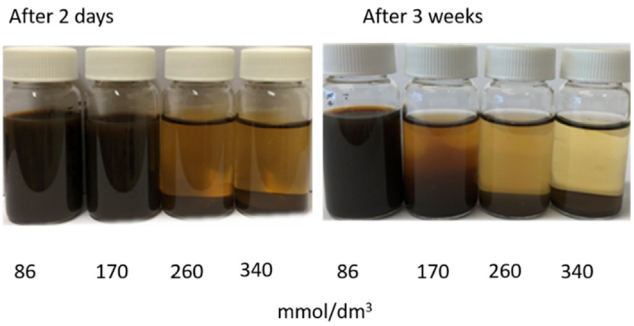

Fig. 3. Destabilization of colloidal hydrochar dispersions (c-CH0.5–86, c-CH0.5–170, c-CH0.5–260 and c-CH0.5–340) illustrated by two photographs: two days and three weeks after salt addition. c-CHX-Z denotes hydrothermal carbonized glucose at concentrations of X mol/dm^3, with electrolyte concentrations of Z mmol/dm^3 of NaCl (aq). The dispersions had been purified by a centrifugation plus redispersion procedure.

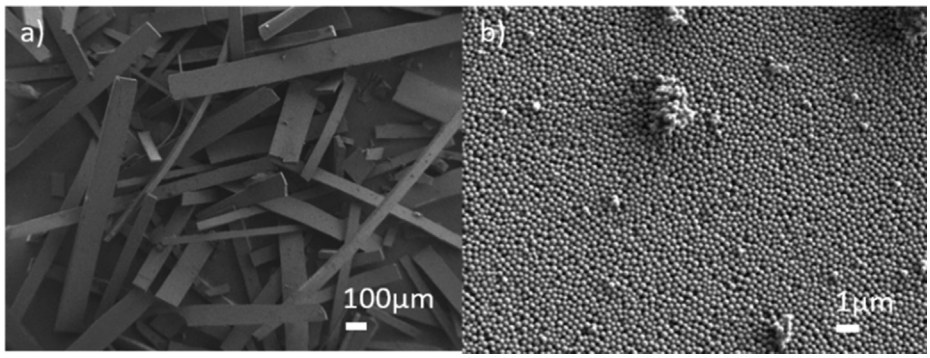

Fig. 4. SEM images of the prismatic rods of carbonized hydrochar particles obtained after 2 h of pyrolysis at 600 °C under a N_2 atmosphere. Sample 1111 was carbonized. (1111 stands for the values of the experimental design matrix, see Table S1 and S2.)

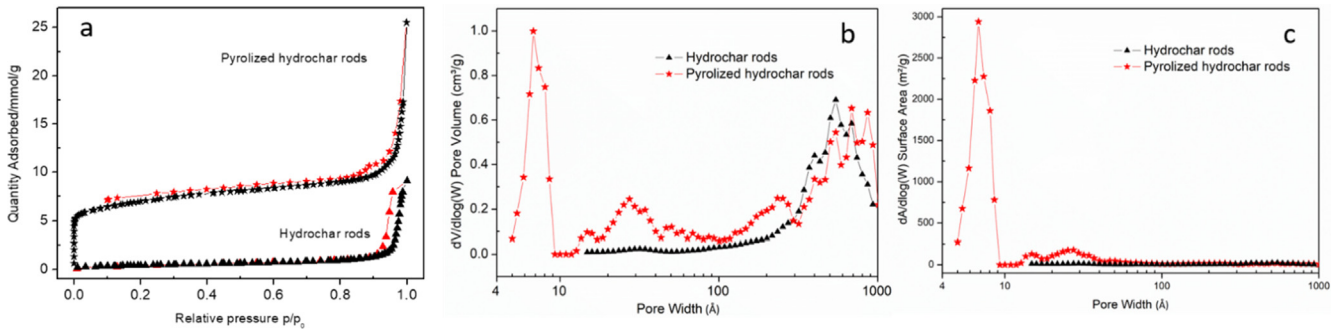

Fig. 5. a) N_2 adsorption and desorption isotherms of the hydrochar before and after pyrolysis (at 800 ∘C for 2 h), recorded at −196 °C, (b) dV/dlog(W) pore volume vs. pore width and (c) dA/dlog(W) surface area vs. pore width.

The specific values for surface areas, pore volumes, and pore surface areas are listed in Table 3. The BET specific surface area of the hydrochar increased from 38 to 563 m^2/g upon pyrolysis, among which the micropores contributed with 285 m^2/g to the surface area. The total pore volume of the pyrolyzed hydrochar was 0.799 cm^3/g, of which a large amount were from the pores smaller than 40 Å. The hydrochar had almost no microporosity, and total pore volume was almost solely from pores > 100 Å.

3.4. Cu_3Si-SiC prepared by reactive infiltration of a Cu-Si alloy in in-situ pyrolyzed hydrochar rods

Sacrificial carbon templates are well studied for the preparation of various materials. [54,55] Here, we used a lesser well-known but flexible method [56] and reactively infiltrated a melted Cu-Si alloy into in-situ pyrolyzed hydrochar rods at 1300 °C. This approach facilitated the formation of a composite material (Cu_3Si-SiC/carbon). The non-reacted carbon in the Cu_3Si-SiC/carbon was still in a spherical form after the reactive high-temperature treatment. The carbon was subsequently removed by calcination in air and Cu_3Si-SiC formed. The processes and outcome are illustrated in Fig. 6. The underlying approach of this method, developed by Chiang et al. [56], builds on wetting by the means of reactive infiltration. Si atoms in the liquid Cu–Si alloy react with C-atoms of the in-situ pyrolyzed carbon forming a layer of SiC that facilitate the wetting and infiltration of the alloy. XRD patterns of the starting Cu-Si alloy, Cu_3Si-SiC/carbon, and Cu_3Si-SiC are shown in Fig. 7. The starting alloy contained Cu_7Si_2 and Si (Fig. 7a). The Cu_3Si-SiC/carbon (Fig. 7b) had lines for SiC showing that Si had reacted with in-situ pyrolyzed hydrochar. The broad diffraction peaks (scattering features) at about 23° and 43° were characteristics of the 002 and 100 reflections of carbon, which were consistent with an amorphous nature of the pyrolyzed hydrochar. After calcination of Cu_3Si-SiC/carbon into Cu_3Si-SiC, the broad peaks in the X-ray diffractogram disappeared as can be seen from Fig. 7c, while signatures of Cu_3Si and some SiO_2 appeared as diffraction lines. [57,58] (The diffractograms of Cu_3Si-SiC/carbon and Cu_3Si-SiC (in Fig. 7) had different relative SiC peak intensities, which showed that non-uniformities were present in the materials.)

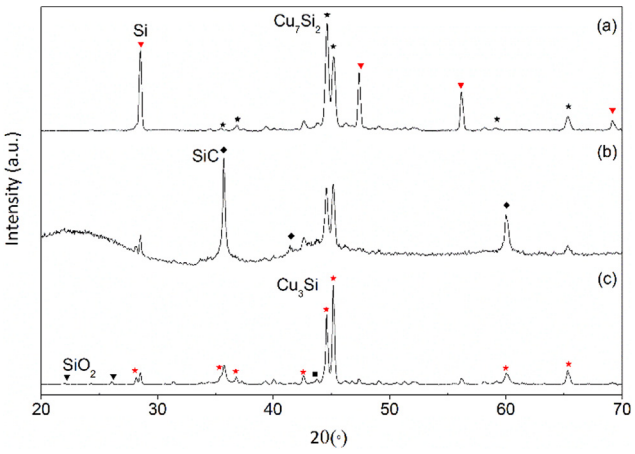

Fig. 7. XRD patterns of a) the Cu-Si alloy used for the reactive infiltration in pyrolyzed hydrochar, b) the alloy as reactively infiltrated Cu_3Si-SiC/carbon and c) the calcined reactively infiltrated Cu_3Si-SiC. A d-CH0.5: alloy (mass) of 1:1.5 were used for reactive infiltration.

To further understand the features of the materials formed upon reactive infiltration, SEM was used. Features in both the Cu_3Si SiC/carbon and the calcined Cu_3Si-SiC were studied, and selected SEM images are displayed in Fig. 8. Organized spherical particles remained in the Cu_3Si-SiC/carbon sample as can be seen from the SEM image in Fig. 8a. The organization of the spherical particles was similar to the one found in the hydrochar-based rods, c.f. Fig. 1-c-e. A solid layer of another material was present on the spherical particles of carbon as shown in the SEM image of the Cu_3Si-SiC/carbon (Fig. 8b). This layer filled the spaces among the spherical particles and formed interconnections. With the XRD results considered, we concluded that this layer and the spherical particles contained SiC and Cu_3Si. After calcination in air, the rod-like macro

Table 3
Surface areas, pore volumes and pore surface of the hydrochar rods and pyrolyzed hydrochar rods of d-CH0.5.

Sample	Surface Area (S) / m^2/g				Total volume in pores (V) / cm^3/g
	S_{BET}	S_{micro}	S_{ex}	S_{pore}	
Hydrochar rods	38	–	44	$15_{(>=14.8Å)}$	0.241
Pyrolyzed hydrochar rods	563	285	278	$490_{(>=5.0Å)}$	0.799

One experiment was conducted for each sample, and the internal error within the experiment is estimated to be ~ 1%.

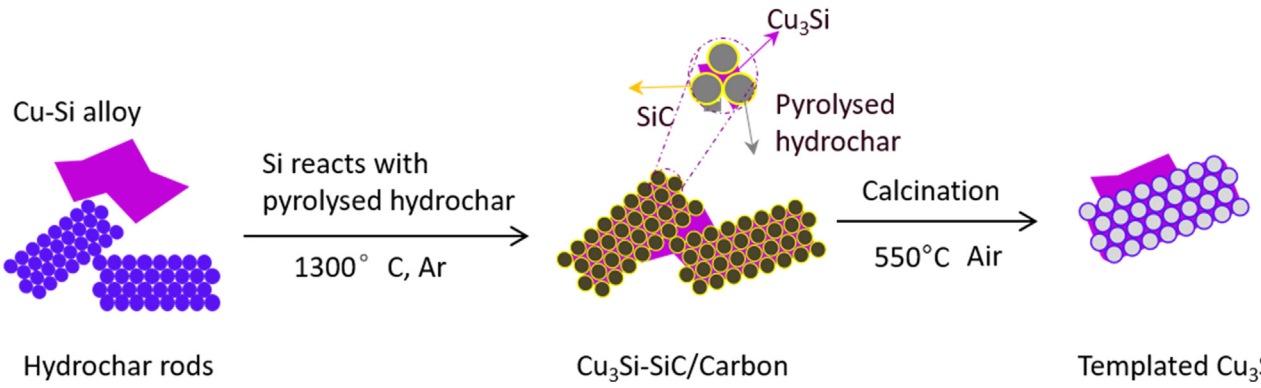

Fig. 6. Schematic representation of the reactive infiltration process used for preparing a Cu_3Si-SiC material from rods of assembled hydrochar by in-situ pyrolysis of hydrochar combined with reactive wetting of a Cu-Si alloy.

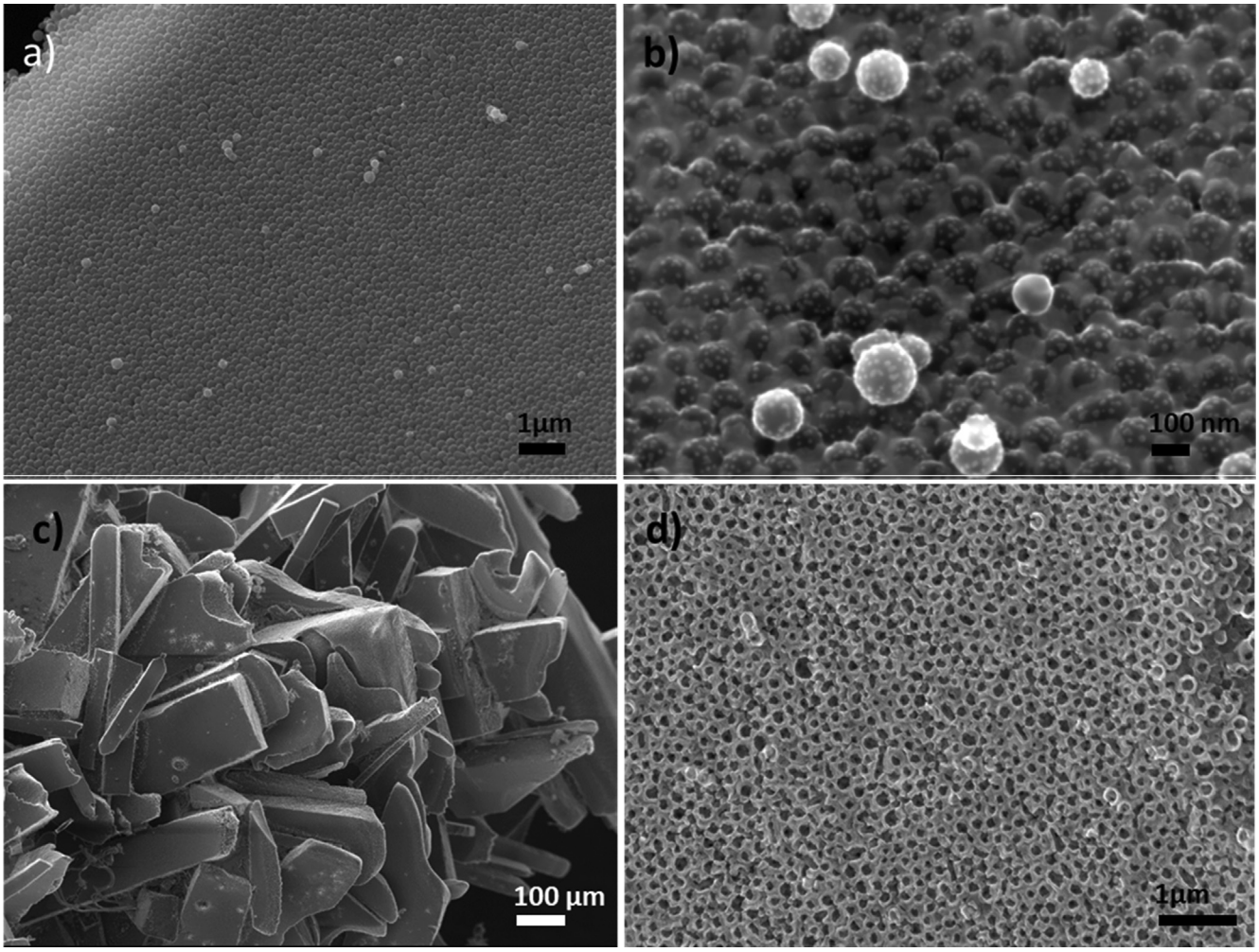

Fig. 8. SEM images of a) and b) the composite sample (Cu_3Si-SiC/carbon) consisting of pyrolyzed hydrochar reactively infiltrated with a Cu-Si alloy; c) and d) Cu_3Si-SiC, the composite sample calcined in air. A hydrochar (d-CH0.5): alloy (mass) = 1:1.5 was used for the reactive infiltration.

morphology prevailed in form of Cu_3Si-SiC as can be seen in the SEM image of Fig. 8c. Note that this image displays the outer part of the Cu_3Si-SiC where the alloy had been exposed to the pyrolysed carbon during the reactive infiltration. There was a layer covering the outer perimeter of the rods. An interconnected and 3D-porous structure formed in Cu_3Si-SiC, as can be seen from the hollow structures in the SEM image of Fig. 8d. By combining the information on the morphology of the particles, XRD and SEM-EDS results (Table S6), we concluded that the remaining framework of Cu_3Si-SiC consisted mainly of SiC and Cu_3Si. This reactive infiltration method could open up the possibility for hydrochar derived alloys with SiC prepared from other biomass like cellulose, hemicellulose, lignin, etc., especially when uniform spherical hydrochar particles can be synthesized by adjusting the hydrothermal conditions; similar alloy structure could be obtained [59,60].

Metal silicides are of interest because of their considerable stability and oxidation resistance, and are relevant for their applications in microelectronics and catalysis. Silicides of copper in specific can be used as catalysts for hydrogenation, chlorosilanes formation, hydrodechlorination and gas etching of silicon [61,62], and due to their semiconducting nature they may be used as electrodes [63], electronic packaging, and as photocatalysts. SiC is used in many applications commercially [64,65], and is actively researched as an alternative support in catalysis [66], as it is highly resilient to aggressive process conditions. We speculate that our approach of reactive infiltration can allow for a control of the shapes, structure and pore size of the metal silicide and SiC, which can enable rapid and controlled uptake of molecules, etc.

4. Conclusions

Macroscopically large rods formed on the evaporation of water from dispersions of uniform colloidal hydrochar particles at the interface of colloidal solution and vapor phase on the inner surface of glass or polypropylene vials at elevated temperatures. The rods formed orthogonally with respect to the moving liquid surface at intermediate pH values and comprised tightly packed hydrochar particles. The rods could be pyrolyzed to carbon without changing the shape of the rods or the spherical shape of the constituting small particles, and the resulting pyrolized carbon was highly porous. As an application example, the long rods were used as templates for the preparation of a tricopper silicide (Cu_3Si)-silicon carbide (SiC)/carbon material and upon calcination a Cu_3Si-SiC material.

The formation of macroscopically large rods from colloidal hydrochar particles (or other carbon-rich colloids) by directed assembly at the glass or polypropylene surface has not been observed before. Nonetheless, it relates well to findings for silica or polymer based colloids for which the theoretical base for under-

standing is reasonably well developed. It was our hypothesis that the domain of formation of rods could be linked to the domain of colloidal stability for the hydrochar particles and this was confirmed by experiments. The colloidal dispersions were electrostatically stable at pH > 3.4 and the rods formed at pH = 4.1 – 9.5. Our application example employed a less known method of reactive infiltration of a Cu-Si alloy into the in-situ pyrolyzed carbon.

Further studies are foreseen of the associated colloidal chemistry of monodisperse and purified particles of hydrochar from other biomass. It would be interesting to understand how long rods, other kinds of directed assemblies, or even colloidal crystals could form and be used as template for reactive infiltration and the formation of Cu_3Si-SiC and other related compositions. Also, studies of the Cu_3Si-SiC, in for example catalysis, could be warranted.

Author contributions

The manuscript was written through contributions of all authors. All authors have given approval to the final version of the manuscript.

CRediT authorship contribution statement

Xia Wang: Methodology, Data curation, Visualization, Writing - original draft. **Wenming Hao:** Methodology, Writing - review & editing. **Peng Zhang:** Methodology, Writing - review & editing. **Anthony E. Szego:** Methodology, Writing - review & editing. **Gunnar Svensson:** Writing - review & editing, Supervision. **Niklas Hedin:** Methodology, Conceptualization, Writing - review & editing, Supervision, Funding acquisition.

Declaration of Competing Interest

The authors declare that they have no known competing financial interests or personal relationships that could have appeared to influence the work reported in this paper.

Acknowledgement

We would like to thank Cheuk-Wai Tai, Anumol Ashok, Jekabs Grins, Girma Gebresenbut for supporting the TEM and reactive infiltration experiments. This project was supported by the EU-MSCA-ETN-GreenCarbon project 721991. Wenming Hao would like to thank the support by the Applied Basic Research Program of Shanxi Province (no. 201801D221127).

Appendix A. Supplementary material

The Supporting Information is available free of charge at xxx.

Supplementary data to this article can be found online at https://doi.org/10.1016/j.jcis.2021.06.016.

References

[1] X. Sun, Y. Li, Colloidal carbon spheres and their core/shell structures with noble-metal nanoparticles, Angew. Chem. Int. Ed. Engl. 43 (2004) 597–601, https://doi.org/10.1002/anie.200352386.
[2] M. Faraday, X. The Bakerian Lecture. —Experimental relations of gold (and other metals) to light, Philos. Trans. R. Soc. 147 (1857) 145–181. DOI: 10.1098/rstl.1857.0011.
[3] J. Park, J. Joo, S.G. Kwon, Y. Jang, T. Hyeon, Synthesis of Monodisperse Spherical Nanocrystals, Angew. Chem. 46 (2007) 4630–4660, https://doi.org/10.1002/anie.200603148.
[4] Y. Xia, Y. Xiong, B. Lim, S.E. Skrabalak, Shape-Controlled Synthesis of Metal Nanocrystals: Simple Chemistry Meets Complex Physics?, Angew. Chem. 48 (2009) 60–103, https://doi.org/10.1002/anie.200802248.
[5] M.-R. Gao, Y.-F. Xu, J. Jiang, S.-H. Yu, Nanostructured metal chalcogenides: synthesis, modification, and applications in energy conversion and storage devices, Chem. Soc. Rev. 42 (2013) 2986–3017, https://doi.org/10.1039/C2CS35310E.
[6] S. Schlücker, Surface-Enhanced Raman Spectroscopy: Concepts and Chemical Applications, Angew. Chem. 53 (2014) 4756–4795, https://doi.org/10.1002/anie.201205748.
[7] S. Guo, S. Zhang, S. Sun, Tuning Nanoparticle Catalysis for the Oxygen Reduction Reaction, Angew. Chem. 52 (2013) 8526–8544, https://doi.org/10.1002/anie.201207186.
[8] K. Saha, S.S. Agasti, C. Kim, X. Li, V.M. Rotello, Gold Nanoparticles in Chemical and Biological Sensing, Chem. Rev. 112 (2012) 2739–2779, https://doi.org/10.1021/cr2001178.
[9] E. Boisselier, D. Astruc, Gold nanoparticles in nanomedicine: preparations, imaging, diagnostics, therapies and toxicity, Chem. Soc. Rev. 38 (2009) 1759–1782, https://doi.org/10.1039/B806051G.
[10] H. Ko, H.-W. Lee, J. Moon, Fabrication of colloidal self-assembled monolayer (SAM) using monodisperse silica and its use as a lithographic mask, Thin Solid Films 447–448 (2004) 638–644, https://doi.org/10.1016/j.tsf.2003.04.001.
[11] A. Van Blaaderen, R. Ruel, P. Wiltzius, Template-directed colloidal crystallization, Nature 385 (1997) 321–324, https://doi.org/10.1038/385321a0.
[12] E. Matijevic, Uniform inorganic colloid dispersions, Achievements and challenges, Langmuir. 10 (1994) 8–16, https://doi.org/10.1021/la00013a003.
[13] M.E. Leunissen, C.G. Christova, A.-P. Hynninen, C.P. Royall, A.I. Campbell, A. Imhof, M. Dijkstra, R. van Roij, A. van Blaaderen, Ionic colloidal crystals of oppositely charged particles, Nature 437 (2005) 235–240, https://doi.org/10.1038/nature03946.
[14] G.H. Bogush, M.A. Tracy, C.F. Zukoski, Preparation of monodisperse silica particles: Control of size and mass fraction, J. Non-Cryst. Solids. 104 (1988) 95–106, https://doi.org/10.1016/0022-3093(88)90187-1.
[15] C.B. Murray, S. Sun, W. Gaschler, H. Doyle, T.A. Betley, C.R. Kagan, Colloidal synthesis of nanocrystals and nanocrystal superlattices, IBM J. Res. Dev. 45 (2001) 47–56, https://doi.org/10.1147/rd.451.0047.
[16] Y. Xia, T.D. Nguyen, M. Yang, B. Lee, A. Santos, P. Podsiadlo, Z. Tang, S.C. Glotzer, N.A. Kotov, Self-assembly of self-limiting monodisperse supraparticles from polydisperse nanoparticles, Nat. Nanotechnol. 6 (2011) 580–587, https://doi.org/10.1038/nnano.2011.121.
[17] L. Antl, J.W. Goodwin, R.D. Hill, R.H. Ottewill, S.M. Owens, S. Papworth, J.A. Waters, The preparation of poly(methyl methacrylate) latices in non-aqueous media, Colloid Surface. 17 (1986) 67–78, https://doi.org/10.1016/0166-6622(86)80187-1.
[18] P. Jiang, J.F. Bertone, V.L. Colvin, A Lost-Wax Approach to Monodisperse Colloids and Their Crystals, Science 291 (2001) 453–457, https://doi.org/10.1126/science.291.5503.453.
[19] C. Burda, X. Chen, R. Narayanan, M.A. El-Sayed, Chemistry and properties of nanocrystals of different shapes, Chem. Rev. 105 (2005) 1025–1102, https://doi.org/10.1021/cr030063a.
[20] B. Dunn, H. Kamath, J.-M. Tarascon, Electrical energy storage for the grid: A battery of choices, Science 334 (2011) 928–935, https://doi.org/10.1126/science.1212741.
[21] A. Kudo, Y. Miseki, Heterogeneous photocatalyst materials for water splitting, Chem. Soc. Rev. 38 (2009) 253–278, https://doi.org/10.1039/b800489g.
[22] X. Chen, S. Shen, L. Guo, S.S. Mao, Semiconductor-based photocatalytic hydrogen generation, Chem. Rev. 110 (2010) 6503–6570, https://doi.org/10.1021/cr1001645.
[23] J. Wencel-Delord, F. Glorius, C-H bond activation enables the rapid construction and late-stage diversification of functional molecules, Nat. Chem. 5 (2013) 369–375, https://doi.org/10.1038/nchem.1607.
[24] P. Sarkar, P.S. Nicholson, Electrophoretic Deposition (EPD): Mechanisms, Kinetics, and Application to Ceramics, J. Am. Ceram. Soc. 79 (1996) 1987–2002, https://doi.org/10.1111/j.1151-2916.1996.tb08929.x.
[25] M. Sevilla, A.B. Fuertes, Chemical and Structural Properties of Carbonaceous Products Obtained by Hydrothermal Carbonization of Saccharides, Chem. Eur. J. 15 (2009) 4195–4203, https://doi.org/10.1002/chem.200802097.
[26] A. Funke, F. Ziegler, Hydrothermal carbonization of biomass: A summary and discussion of chemical mechanisms for process engineering, Biofuel Bioprod. Bior. 4 (2010) 160–177, https://doi.org/10.1002/bbb.198.
[27] C. Yao, Y. Shin, L.-Q. Wang, C.F. Windisch Jr., W.D. Samuels, B.W. Arey, C. Wang, W.M. Risen Jr., G.J. Exarhos, Hydrothermal dehydration of aqueous fructose solutions in a closed system, J. Phys. Chem. C. 111 (2007) 15141–15145, https://doi.org/10.1021/jp074188l.
[28] T.R. Carlson, G.A. Tompsett, W.C. Conner, G.W. Huber, Aromatic production from catalytic fast pyrolysis of biomass-derived feedstocks, Top. Catal. 52 (2009) 241–252, https://doi.org/10.1007/s11244-008-9160-6.
[29] N. Baccile, G. Laurent, F. Babonneau, F. Fayon, M.-M. Titirici, M. Antonietti, Structural Characterization of Hydrothermal Carbon Spheres by Advanced Solid-State MAS 13C NMR Investigations, J. Phys. Chem. C. 113 (2009) 9644–9654, https://doi.org/10.1021/jp901582x.
[30] M. Sevilla, A.B. Fuertes, The production of carbon materials by hydrothermal carbonization of cellulose, Carbon 47 (2009) 2281–2289, https://doi.org/10.1016/j.carbon.2009.04.026.
[31] Q. Wang, H. Li, L. Chen, X. Huang, Monodispersed hard carbon spherules with uniform nanopores, Carbon 39 (2001) 2211–2214, https://doi.org/10.1016/S0008-6223(01)00040-9.

[32] M. Zheng, Y. Liu, Y. Xiao, Y. Zhu, Q. Guan, D. Yuan, J. Zhang, An Easy Catalyst-Free Hydrothermal Method to Prepare Monodisperse Carbon Microspheres on a Large Scale, J. Phys. Chem. C. 113 (2009) 8455–8459, https://doi.org/10.1021/jp811356a.
[33] Q. Zhao, S. Tao, X. Miao, Y. Zhu, A green, rapid, scalable and versatile hydrothermal strategy to fabricate monodisperse carbon spheres with tunable micrometer size and hierarchical porosity, Chem. Eng. J. 372 (2019) 1164–1173, https://doi.org/10.1016/j.cej.2019.05.014.
[34] A. Fojtik, H. Weller, U. Koch, A. Henglein, Photo-Chemistry of Colloidal Metal Sulfides 8. Photo-Physics of Extremely Small CdS Particles: Q-State CdS and Magic Agglomeration Numbers, Berichte Der Bunsengesellschaft Für Physikalische Chemie. 88 (1984) 969–977, https://doi.org/10.1002/bbpc.19840881010.
[35] S. Rakers, L.F. Chi, H. Fuchs, Influence of the Evaporation Rate on the Packing Order of Polydisperse Latex Monofilms, Langmuir 13 (1997) 7121–7124, https://doi.org/10.1021/la970757c.
[36] W.B. Russel, Tunable colloidal crystals, Nature 421 (2003) 490–491, https://doi.org/10.1038/421490a.
[37] E. Adachi, A.S. Dimitrov, K. Nagayama, Stripe Patterns Formed on a Glass Surface during Droplet Evaporation, Langmuir 11 (1995) 1057–1060, https://doi.org/10.1021/la00004a003.
[38] O. Giraldo, J.P. Durand, H. Ramanan, K. Laubernds, S.L. Suib, M. Tsapatsis, S.L. Brock, M. Marquez, Dynamic Organization of Inorganic Nanoparticles into Periodic Micrometer-Scale Patterns, Angew. Chem. Int. Ed. 42 (2003) 2905–2909, https://doi.org/10.1002/anie.200250712.
[39] E.C.H. Ng, K.M. Chin, C.C. Wong, Controlling Inplane Orientation of a Monolayer Colloidal Crystal by Meniscus Pinning, Langmuir 27 (2011) 2244–2249, https://doi.org/10.1021/la104265b.
[40] J. Xu, J. Xia, Z. Lin, Evaporation-Induced Self-Assembly of Nanoparticles from a Sphere-on-Flat Geometry, Angew. Chem. Int. Ed. 46 (2007) 1860–1863, https://doi.org/10.1002/anie.200604540.
[41] B.D. Edmonstone, O.K. Matar, R.V. Craster, Coating of an inclined plane in the presence of insoluble surfactant, J. Colloid Interface Sci. 287 (2005) 261–272, https://doi.org/10.1016/j.jcis.2005.01.105.
[42] D.K.N. Sinz, M. Hanyak, A.A. Darhuber, Immiscible surfactant droplets on thin liquid films: Spreading dynamics, subphase expulsion and oscillatory instabilities, J. Colloid Interface Sci. 364 (2011) 519–529, https://doi.org/10.1016/j.jcis.2011.08.055.
[43] J.J. Ramsden, R.H. Ottewill, The stability of superspheres, Proc. R. Soc. Lond. A. 413 (1987) 407–414, https://doi.org/10.1098/rspa.1987.0122.
[44] A.A. Shah, M. Ganesan, J. Jocz, M.J. Solomon, Direct Current Electric Field Assembly of Colloidal Crystals Displaying Reversible Structural Color, ACS Nano 8 (2014) 8095–8103, https://doi.org/10.1021/nn502107a.
[45] R. Demir-Cakan, N. Baccile, M. Antonietti, M.-M. Titirici, Carboxylate-Rich Carbonaceous Materials via One-Step Hydrothermal Carbonization of Glucose in the Presence of Acrylic Acid, Chem. Mater. 21 (2009) 484–490, https://doi.org/10.1021/cm802141h.
[46] T. Yokoi, J. Wakabayashi, Y. Otsuka, W. Fan, M. Iwama, R. Watanabe, K. Aramaki, A. Shimojima, T. Tatsumi, T. Okubo, Mechanism of Formation of Uniform-Sized Silica Nanospheres Catalyzed by Basic Amino Acids, Chem. Mater. 21 (2009) 3719–3729, https://doi.org/10.1021/cm900993b.
[47] Z. Liu, Y. Song, D. Li, Detecting zeta potential of polydimethylsiloxane (PDMS) in electrolyte solutions with atomic force microscope, J. Colloid Interface Sci. 578 (2020) 116–123, https://doi.org/10.1016/j.jcis.2020.05.061.
[48] S. Tcholakova, N.D. Denkov, D. Sidzhakova, I.B. Ivanov, B. Campbell, Effects of Electrolyte Concentration and pH on the Coalescence Stability of β-Lactoglobulin Emulsions: Experiment and Interpretation, Langmuir 21 (2005) 4842–4855, https://doi.org/10.1021/la046891w.
[49] Y. Gong, L. Xie, H. Li, Y. Wang, Sustainable and scalable production of monodisperse and highly uniform colloidal carbonaceous spheres using sodium polyacrylate as the dispersant, Chem. Commun. 50 (2014) 12633–12636, https://doi.org/10.1039/C4CC04998E.
[50] E.J.W. Verwey, J.Th.G. Overbeek, Theory of the stability of lyophobic colloids: the interaction of sol particles having and electric double layer, Elsevier, Amsterdam, 1948.
[51] P. Mukerjee, C.C. Chan, Effects of High Salt Concentrations on the Micellization of Octyl Glucoside: Salting-Out of Monomers and Electrolyte Effects on the Micelle−Water Interfacial Tension1, Langmuir 18 (2002) 5375–5381, https://doi.org/10.1021/la020059e.
[52] A.B. Jódar-Reyes, A. Martín-Rodríguez, J.L. Ortega-Vinuesa, Effect of the ionic surfactant concentration on the stabilization/destabilization of polystyrene colloidal particles, J. Colloid Interface Sci. 298 (2006) 248–257, https://doi.org/10.1016/j.jcis.2005.12.035.
[53] S. Haddadi, M. Skepö, P. Jannasch, S. Manner, J. Forsman, Building polymer-like clusters from colloidal particles with isotropic interactions, in aqueous solution, J. Colloid Interface Sci. 581 (2021) 669–681, https://doi.org/10.1016/j.jcis.2020.07.150.
[54] H. Tüysüz, E.L. Salabaş, C. Weidenthaler, F. Schüth, Synthesis and Magnetic Investigation of Ordered Mesoporous Two-Line Ferrihydrite, J. Am. Chem. Soc. 130 (2008) 280–287, https://doi.org/10.1021/ja075528j.
[55] D. Gu, F. Schüth, Synthesis of non-siliceous mesoporous oxides, Chem. Soc. Rev. 43 (2014) 313–344, https://doi.org/10.1039/c3cs60155b.
[56] Y.-M. Chiang, J.-R. Lee, L. Hozer, Method for Producing an Article by Pressureless Reactive Infiltration, 5,509,555, 1996. U.S.
[57] P.K. Ng, B. Fisher, K.B. Low, A. Joshi-Imre, M. Bode, C.M. Lilley, Comparison between bulk and nanoscale copper-silicide: Experimental studies on the crystallography, chemical, and oxidation of copper-silicide nanowires on Si (001), J. Appl. Phys. 111 (2012), https://doi.org/10.1063/1.4712536 104301.
[58] C.S. Liu, L.J. Chen, Room-temperature oxidation of silicon in the presence of Cu3Si, Thin Solid Films 262 (1995) 187–198, https://doi.org/10.1016/0040-6090(95)05814-1.
[59] T. Wang, Y. Zhai, Y. Zhu, C. Li, G. Zeng, A review of the hydrothermal carbonization of biomass waste for hydrochar formation: Process conditions, fundamentals, and physicochemical properties, Renew. Sustain. Energy Rev. 90 (2018) 223–247, https://doi.org/10.1016/j.rser.2018.03.071.
[60] H. Mao, X. Chen, R. Huang, M. Chen, R. Yang, P. Lan, M. Zhou, F. Zhang, Y. Yang, X. Zhou, Fast preparation of carbon spheres from enzymatic hydrolysis lignin: Effects of hydrothermal carbonization conditions, Sci. Rep. 8 (2018) 9501, https://doi.org/10.1038/s41598-018-27777-4.
[61] A.H. Reader, A.H. van Ommen, P.J.W. Weijs, R.A.M. Wolters, D.J. Oostra, Transition metal silicides in silicon technology, Rep. Prog. Phys. 56 (1993) 1397–1467, https://doi.org/10.1088/0034-4885/56/11/002.
[62] L.J. Chen, Metal silicides: An integral part of microelectronics, JOM. 57 (2005) 24–30, https://doi.org/10.1007/s11837-005-0111-4.
[63] H.-J. Ahn, Y.-S. Kim, W.B. Kim, Y.-E. Sung, T.-Y. Seong, Formation and characterization of Cu–Si nanocomposite electrodes for rechargeable Li batteries, J. Power Sources. 163 (2006) 211–214, https://doi.org/10.1016/j.jpowsour.2005.12.077.
[64] W.-J. Ding, J.-M. Yan, W.-D. Xiao, Hydrogenation of Silicon Tetrachloride in the Presence of Silicon: Thermodynamic and Experimental Investigation, Ind. Eng. Chem. Res. 53 (2014) 10943–10953, https://doi.org/10.1021/ie5019222.
[65] X. Chen, C. Liang, Transition metal silicides: fundamentals, preparation and catalytic applications, Catal. Sci. Technol. 9 (2019) 4785–4820, https://doi.org/10.1039/C9CY00533A.
[66] M.-Y. Li, W.-D. Lu, L. He, F. Schüth, A.-H. Lu, Tailoring the Surface Structure of Silicon Carbide Support for Copper Catalyzed Ethanol Dehydrogenation, ChemCatChem 11 (2019) 481–487, https://doi.org/10.1002/cctc.201801742.